HHS Public Access

Author manuscript

Cancer Immunol Res. Author manuscript; available in PMC 2021 August 01.

Published in final edited form as:

Cancer Immunol Res. 2021 February ; 9(2): 156–169. doi:10.1158/2326-6066.CIR-20-0315.

KIR3DL3 is an inhibitory receptor for HHLA2 that mediates an alternative immunoinhibitory pathway to PD1

Rupal S. Bhatt[1,*], **Abdulla Berjis**[#2], **Julie C. Konge**[#1], **Kathleen M. Mahoney**[#1,2], **Alyssa N. Klee**[#2], **Samuel S. Freeman**[2,3], **Chun-Hau Chen**[1], **Opeyemi A. Jegede**[4], **Paul J. Catalano**[4], **Jean-Christophe Pignon**[5], **Maura Sticco-Ivins**[5], **Baogong Zhu**[2], **Ping Hua**[2], **Jo Soden**[6], **Jie Zhu**[7], **David F. McDermott**[1], **Antonio R. Arulanandam**[2], **Sabina Signoretti**[5,8], **Gordon J. Freeman**[2,*]

[1]Department of Medicine, Division of Hematology and Oncology, Beth Israel Deaconess Medical Center, Boston, Massachusetts

[2]Department of Medical Oncology, Dana-Farber Cancer Institute, Harvard Medical School, Boston, Massachusetts

[3]Broad Institute of MIT and Harvard, Cambridge, Massachusetts

[4]Department of Data Sciences, Dana-Farber Cancer Institute, Boston, Massachusetts

[5]Department of Pathology, Brigham and Women's Hospital, Harvard Medical School, Boston, Massachusetts

[6]Retrogenix, Chinley, High Peak, United Kingdom

[7]BPS Bioscience, San Diego, California

[8]Department of Oncologic Pathology, Dana-Farber Cancer Institute, Harvard Medical School, Boston, Massachusetts

[#] These authors contributed equally to this work.

Abstract

Blockade of the PD1 pathway is a broadly effective cancer therapy, but additional immune inhibitory pathways contribute to tumor immune evasion. HERV-H LTR-associating 2 (HHLA2; also known as B7H5 and B7H7) is a member of the B7 family of immunoregulatory ligands that mediates costimulatory effects through its interaction with the CD28 family member transmembrane and immunoglobulin domain containing 2 (TMIGD2). However, HHLA2 is also

[*]Corresponding Authors Rupal S.Bhatt, MD/PhD, Beth Israel Deaconess Medical Center, 330 Brookline Avenue, Boston, MA 02213; Phone: 617-735-2062; Fax: 617-735-2060; rbhatt@bidmc.harvard.edu; Gordon J. Freeman, PhD, Dana-Farber Cancer Institute, 450 Brookline Ave, Boston, MA 02215; Phone: 617-632-4585; Fax:617-632-5167; gordon_freeman@dfci.harvard.edu.

Conflicts of interest: GJF has patents/pending royalties on the PD1/PDL1 pathway from Roche, Merck MSD, Bristol-Myers-Squibb, Merck KGA, Boehringer-Ingelheim, AstraZeneca, Dako, Leica, Mayo Clinic, and Novartis. GJF has served on advisory boards for Roche, Bristol-Myers-Squibb, Xios, Origimed, Triursus, iTeos, NextPoint, IgM, and Jubilant. GJF has equity in Nextpoint, Triursus, Xios, and IgM. GJF and ARA have patent applications on HHLA2 and KIR3DL3 blockade for cancer immunotherapy. ARA has equity in Nextpoint. GJF and ARA are co-founders of Nextpoint Therapeutics. KMM and GJF report receiving research grants from Bristol-Myers Squibb. SS reports receiving commercial research grants from Bristol-Myers Squibb, AstraZeneca, and Exelixis; is a consultant/advisory board member for Merck, AstraZeneca, Bristol-Myers Squibb, AACR, and NCI; and receives royalties from Biogenex. DFM reports receiving research grants from BMS, Merck, Alkermes Inc, Genentech, Pfizer, Exelixis, X4 Pharma and honoraria from BMS, Pfizer, Merck, and Alkermes Inc.

been known to have inhibitory effects on T cells. Here, we report that we have identified killer cell immunoglobulin-like receptor, three immunoglobulin domains and long cytoplasmic tail 3 (KIR3DL3) as an inhibitory receptor for HHLA2 in T cells and natural killer (NK) cells and have generated HHLA2 and KIR3DL3 antibodies that block the immune-inhibitory activity of HHLA2, preserving the costimulatory signal. It is known that HHLA2 is frequently expressed in several tumor types, including clear cell renal cell carcinoma (ccRCC). We found that HHLA2 expression was non-overlapping with PDL1 expression in ccRCC, suggesting that HHLA2 mediates a mechanism of tumor immune evasion that is independent from PDL1. Blockade of both PD1 and KIR3DL3 pathways may be a more effective way to reverse tumor immune evasion.

Keywords

HHLA2; KIR3DL3; immune checkpoint; renal cancer; costimulation

Introduction

Immune checkpoint blockade (ICB) has revolutionized the field of cancer therapy (1–3). Modulation of the immune-inhibitory versus immune-stimulatory functions of T cells through ICB is effective in multiple cancer types including melanoma, lung cancer, bladder cancer, and renal cancer, but a significant percentage of patients do not respond to this treatment and many of the patients that do respond eventually develop resistance (4–6). There is a critical unmet need to find additional immune pathways that are non-redundant with the PD1 pathway.

HERV-H LTR-associating 2 (HHLA2; also known as B7H5 and B7H7) is a B7 family member that is highly expressed in several solid and hematologic cancers including primary human renal cell carcinoma (RCC) by immunohistochemistry and based upon RNA-Seq data from The Cancer Genome Atlas (TCGA) database (7–10). HHLA2 can have either a costimulatory or a coinhibitory effect on T-cell activation (11–13). The costimulatory effect of HHLA2 on T cells and NK cells is mediated through the CD28 family member transmembrane and immunoglobulin domain containing 2 (TMIGD2; also known as CD28H and IGPR1), but the coinhibitory receptor is unknown (11, 13–15). In this study we have identified killer cell immunoglobulin like receptor, three immunoglobulin domains and long cytoplasmic tail 3 (KIR3DL3) as a coinhibitory receptor for HHLA2 and confirmed the costimulatory activity of TMIGD2.

KIR3DL3 is a largely uncharacterized member of the KIR family of inhibitory receptors that contain an immunoreceptor tyrosine-based inhibitory motif (ITIM)(16–18). Both the receptors and ligands of the HHLA2–KIR3DL3–TMIGD2 pathway are expressed in primates and not found in multiple other mammals including rodents, which is unique within the B7 and CD28 families (19). We found that KIR3DL3 was expressed on a subpopulation of activated T cells and some NK cells and inhibited their function.

We generated monoclonal antibodies (mAbs) against HHLA2 and KIR3DL3 that specifically blocked the KIR3DL3 inhibitory activity while preserving the TMIGD2 immune-stimulatory effects of HHLA2. Our findings suggest that the HHLA2 immune

checkpoint has parallels to the B7–CD28/CTLA4 pathway, where the B7–CD28 interaction is stimulatory and the B7–CTLA4 interaction is inhibitory (2). Thus, HHLA2 could have immune-inhibitory effects or immune-stimulatory effects depending on its receptor interaction. Given that we showed that HHLA2 expression in clear cell RCC (ccRCC) was distinct from PDL1 expression, the data presented in this paper suggest that targeting the HHLA2–KIR3DL3 inhibitory checkpoint pathway alone or in combination with PD1 blockade could provide a way to treat patients with metastatic cancer.

Materials and Methods

Expression screen to identify additional receptors for HHLA2

Receptors for HHLA2 were identified using cell microarray technology at Retrogenix, High Peak, UK. A library of approximately 5,500 full-length cDNA clones covering more than 3,500 different plasma membrane proteins was arrayed in duplicate across 13 microarray slides (“slide sets”). Human HEK293 cells were grown above the cDNA clones and reverse transfected. A positive control expression vector (pIRES-hEGFR-IRES-ZsGreen1) was spotted in quadruplicate on every slide and was used to ensure that a minimal threshold of transfection efficiency had been achieved or exceeded on every slide. The resultant cell microarrays were evaluated for binding to soluble human HHLA2-mIgG2a fusion protein (see Recombinant HHLA2-mIgG2a generation).

Human HHLA2-mIgG2a fusion protein was added to fixed cell microarray slides at a 20 μg/ml concentration, and binding interactions were detected with AF647-conjugated goat anti-mouse IgG (H+L) (Life Technologies; cat. #A21235). Two replicate slides were screened for each of the 13 slide sets. Fluorescent images were analyzed and quantitated (for transfection efficiency) using ImageQuant software (GE). A protein ‘hit’ was defined as duplicate spots showing a raised fluorescence signal compared with background levels. This was achieved by visual inspection using the images gridded on the ImageQuant software.

To determine which hit(s), if any, were reproducible and specific to human HHLA2, vectors encoding all library screening hits, plus all 13 KIR receptors, were arrayed and expressed in HEK293 cells on new slides. Two replicate slides were screened with soluble HHLA2-mIgG2a, using the doses and incubation conditions used in the library screens or appropriate positive and negative control treatments (n = 2 slides per treatment).

KIR3DL3 antibodies were screened for KIR3DL3 specificity and lack of reactivity with other KIR family members as follows: Replicate microarray slides expressing a complete KIR family cDNA panel (Retrogenix) were fixed and blocked with buffer containing PBS/0.5% BSA and incubated for 1 hour at room temperature with individual KIR3DL3 mAb hybridoma supernatants at 1:5, 1:25 and 1:250 dilutions in PBS/0.1% BSA. Cell arrays were washed with PBS and incubated for 1 hour at room temperature in PBS/0.1% BSA containing AF647-conjugated goat anti-mouse IgG (H+L) (Life Technologies; cat. #A21235). Slides were washed with PBS, dried, and imaged for ZsGreen1 and AF647 fluorescence. HHLA2-mIgG2a (20 μg/ml) was used as a positive control to detect binding to KIR3DL3 and TMIGD2 on the spotted array.

Cell lines and cell culture

Raji cell line (ATCC CCL-86, 2019), Jurkat (clone E6–1, 2009) (ATCC TIB-152), CHO-K1 (ATCC CCL-61, 2016), A498 (ATCC HTB-44, 2018), 786-O (ATCC CRL-1932, 2018), K562 (ATCC CCL-243, 2018) NK-92 MI (ATCC CRL-2408, 2019), NIH/3T3 (ATCC CRL-1658, 1988) and Sp2/0-Ag14 (ATCC CRL-8287, 1994) cells were obtained from the American Type Culture Collection (ATCC, Manassas, VA, USA). The CHOK1 cells expressing anti-CD3 scFV (BPS Bioscience 60539), Jurkat cells expressing the NFAT reporter (Luc) (BPS Bioscience 60621) and Jurkat cells expressing IL2 reporter (Luc) (BPS Bioscience 60481) were purchased from BPS Bioscience (BPS Bioscience, San Diego, CA, USA).

786-O, A498, Raji, Jurkat and K562 cells were cultured at 37°C with 5% CO_2 in RPMI1640 medium (Life Technologies; cat. #A10491–01) supplemented with 10% fetal bovine serum (FBS; Life Technologies; cat. #26140–079), 1% Gluta-Max (Life Technologies; cat. #35050–061), 1% Penicillin/Streptomycin (Hyclone; cat. #SV30010.01). Sp2/0-Ag14 and hybridoma cells were cultured at 37°C with 10% CO_2 in DMEM medium (Life Technologies; cat. #11995–065) supplemented with 10% FBS, 1% Gluta-Max, 1% Penicillin/Streptomycin. NIH/3T3 cells were cultured at 37°C with 10% CO_2 in DMEM/F12 medium (Life Technologies; cat. #10565–042) supplemented with 10% FBS and 1% Penicillin/Streptomycin. 300.19 (CVCL_6238) were from Naomi Rosenberg, Tufts Medical School and were cultured at 37°C with 5% CO_2 in RPMI1640 medium supplemented with 10% FBS, 1% Gluta-Max, 1% Penicillin/Streptomycin and 50×10^{-6} betamercaptoethanol. NK-92MI cells were cultured at 37°C with 5% CO_2 using X-VIVO 15 Serum-free Hematopoietic Cell Medium (Lonza; cat. #04–418Q) supplemented with 10% FBS (and supplemented with 10% Human serum (Sigma Aldrich; cat. #H3667–100ML) and 1% Penicillin/Streptomycin. Where indicated, cells were treated with IFNγ (R&D; cat. #285-IF/CF; 10 ng/ml), IL10 (R&D; cat. #1064-IF/CF; 10 ng/ml) or TGFβ1 (R&D; cat. #4454-BH; 10 ng/ml). CHO-K1 cells were incubated at 37°C with 5% CO_2 in Ham's F-12 medium (Hyclone; cat. #SH30526.01) supplemented with 10% FBS and 1% Penicillin/Streptomycin.

All ATCC derived cell lines were cultured for fewer than 25 passages and were not reauthenticated upon receipt from ATCC. Raji-HHLA2-B2M knockout cells were verified as Raji by short tandem repeat (STR) analysis (ATCC). K562, 300, NIH/3T3, Raji, Jurkat and CHO-K1 parental and related engineered stable cell lines were screened for mycoplasma and verified to be negative using the MycoAlert Mycoplasma Detection Kit (Lonza; cat. #LT07–118) or Venor GeM Mycoplasma Detection Kit (Sigma-Aldrich; cat. #MP0025).

Plasmid construction

CHO cells expressing cell-surface anti-CD3 scFV, a membrane-anchored chimeric antibody as a T-cell receptor (TCR) activator, were constructed by fusing the single-chain variable fragment (scFv) of the human CD3 mAb OKT3 to the C-terminal domain (amino acids 113–220) of mouse CD8α (accession number: NP_001074579.1). The DNA sequence encoding the TCR activator was synthesized and inserted into pIRES-hyg3 vector (ClonTech; cat. #631620) to make the construct TCRa_pIREShyg3. The NFAT reporter contains a firefly luciferase gene under the control of four copies of the NFAT response element followed by a

minimal promoter. The IL2 reporter contains a firefly luciferase gene under the control of an endogenous IL2 promoter. The DNA sequence encoding the reporters was inserted into pcDNA 3.1 to generate NFAT-Luc-pcDNA and IL2-Luc-pcDNA. The DNA sequence of human HHLA2 (accession number: NM_009003), TMIGD2 (accession number: NM_144615) and KIR3DL3 (Genbank accession number BC143802.1 corresponding to KIR3DL3*00402 allele) were synthesized and inserted into pIRES-Hyg3 or pIRES-Neo3 (ClonTech; cat. #631621) or pEF-Puro.

Generation of stable cell lines

Jurkat cells (clone E6–1) were co-transfected sequentially with NFAT_Luc_pcDNA and TMIGD2_pIREShyg3 by electroporation (BPS Bioscience; cat. #60621). Stable clones were generated by hygromycin (200 μg/ml) (Invitrogen; cat. #10687010) and geneticin (1000 μg/ml) (Life Technologies; cat. #11811031) double selection and limiting dilution. The transfectants were selected in hygromycin, sorted by flow cytometry using TMIGD2 antibody (R&D; cat. #FAB83162), subcloned and were maintained with complete cell culture medium supplemented with hygromycin (200 μg/ml) and G418 (1000 μg/ml).

Jurkat cells (clone E6–1) expressing IL2_promoter Luc_pcDNA (BPS Bioscience; cat. #60481) were transfected with KIR3DL3 (pEF-Puro) by electroporation. The transfectants were selected in media containing puromycin (0.25 μg/ml) (InvivoGen ant-pr-1) and geneticin (1000 μg/ml, ant-gn-1) double selection and limiting dilution and sorted by flow cytometry using KIR3DL3 antibody (R&D; MAB8919). The chosen stable cell clone was maintained with complete cell culture medium supplemented with puromycin (0.25 μg/ml) and geneticin (1000 μg/ml).

CHO-K1 cells were co-transfected sequentially with TCRa_pIREShyg3 and HHLA2_pIRESneo3 by Lipofectamine 2000 using the manufacturer's protocol (Invitrogen). Stable clones were generated by hygromycin (1000 μg/ml) and geneticin (500 μg/ml) double selection and limiting dilution. The stable cell clone was maintained with CHO-K1 culture medium supplemented with hygromycin and geneticin.

sgRNA targeting the human β2-microglobulin gene (5'-GCTACTCTCTCTTTCTGGCC) was ordered from Synthego with 2'-O-methyl 3' phosphorothionate modification in the first and last 3 nucleotides. 2 μl of 66.88 μM of Cas9 Nuclease (Aldevron, SpyFi Cas9 Nuclease 9214–0.25MG) was mixed with 3 μl of 100 μM sgRNA. Cas9 Nuclease and sgRNA were incubated at room temperature for 20 minutes. Raji cells were electroporated with Cas9 RNP using Lonza 4D Nucleofector following Lonza recommended setup for Raji cells. Raji cells were cultured for 48 hours, and wild-type and β2-microglobulin knock-out Raji cells were stained on ice for 30 minutes with either APC-conjugated anti-human β2-microglobulin antibody (Biolegend; cat #395711) or APC mouse IgG1(Biolegend; cat. #400119). β2-microglobulin knock-out cells were sorted based on the gating of the wild-type and isotype control.

β2-microglobulin–negative cells were cultured and re-sorted multiple times as described above until a pure β2-microglobulin negative cell population was obtained.

Recombinant HHLA2-mIgG2a generation

The coding region of human HHLA2 was PCR-amplified using the primers 5'-TGTTCTGCACAAGACA-3' (sense primer located just 5' of ATG start) and 5'-GTAAGGATGCAGGTCATGAGT-3' (anti-sense primer located just 3' to stop codon) and introduced into the pEF6 vector (Thermo Fisher; cat. #K961020) by TA cloning.

The HHLA2-mIgG2a fusion protein was made by fusing cDNA's for the HHLA2 extracellular domain to the mouse IgG2a hinge and Fc domains (with mutations to reduce binding to Fc receptors) and cloning into the pEF6 vector. The construct was introduced into CHO cells and HHLA2-mIgG2a fusion protein was purified by affinity chromatography on a protein G column.

Antibody generation

KIR3DL3 mAbs: Human KIR3DL3 cDNA – pEF-Puro plasmid and KIR3DL3 transfected 3T3 or 300.19 cells were produced and utilized to immunize mice for the derivation of KIR3DL3 mouse monoclonal antibodies. Five mice (Balb/c; C57Bl/6; Swiss-Webster), 4–6 weeks old, were obtained from Charles River Laboratories (Wilmington, MA). All animals were acquired and maintained according to the guidelines of the Institutional Animal Care and Use Committee of Harvard Standing Committee on Animals. Mice were primed in the tibialis muscles with a pre-injection of 100 μl of 10 mM cardiotoxin diluted in 0.9% saline (Naja nigricollis venom; Latoxan Laboratories, France) five days prior to an intramuscular injection of plasmid DNA. The mice were anesthetized and two hundred micrograms of cDNA suspended in 0.9% saline was injected into both tibialis muscles (100 μl each). The cardiotoxin pre-treatment and cDNA boost was repeated on days 14 and day 28. Five weeks later the mice were immunized with KIR3DL3 transfected 300.19 cells in PBS. Two weeks later the mice were immunized with KIR3DL3 transfected NIH-3T3 cells in PBS. Ten days later mice were bled and serum KIR3DL3 mAb titers were evaluated on KIR3DL3 transfected versus untransfected cells by flow cytometry. BALB/c mouse animal #2 that showed the highest serum KIR3DL3 mAb titers was selected for fusion. Five weeks after the previous immunization, mouse #2 was boosted with KIR3DL3 transfected NIH-3T3 cells in PBS and the fusion was performed 4 days later. The harvested spleen and lymph nodes were made into a cell suspension and then washed with DMEM. The spleen/lymph node cells were counted and mixed with SP 2/0 myeloma cells using a spleen:myeloma ratio of 2:1. Cells were fused with polyethylene glycol 1450 and distributed in eight 96-well tissue culture plates in hybridoma media supplemented with hypoxanthine-aminopterin-thymidine (Gibco; cat. #21060017). Between 10 and 21 days after fusion, hybridoma colonies became visible and culture supernatants were harvested and screened by flow cytometry on 300.19 cells transfected with KIR3DL3 cDNA and lack of reactivity on untransfected 300.19 cells.

HHLA2 mAbs: BALB/c mice were primed with 50 μg of recombinant HHLA2-mIg2a in complete Freund's adjuvant by subcutaneous injection. Two boosts, 14 days apart were performed with 50 μg of recombinant HHLA2-mIgG2a and then 42 days later boosted with another round of recombinant HHLA2-mIgG2a in addition to denatured (boiled) HHLA2-mIgG2a in incomplete Freund's adjuvant by intraperitoneal injection. Spleen and lymph node cells from mice that showed the highest HHLA2 antibody titers by flow cytometry

using 293T cells transiently transfected with HHLA2 or vector were fused to SP2/0 myeloma cells using polyethylene glycol mediated fusion. Hybridoma supernatants were screened by flow cytometry on 300.19 cells transfected with HHLA2 cDNA and lack of reactivity on untransfected 300.19 cells.

HHLA2 binding to KIR3DL3 blocking assay

The indicated concentrations of KIR3DL3 mAbs were pre-incubated with KIR3DL3 transfected 300.19 cells for 30 minutes at 4°C. HHLA2-mouse IgG2a (mutated at IgG2a L235E, E318A, K320A, K322A) (25 μl of 10 μg/ml) was added and incubation continued for 30 minutes at 4°C. Cells were washed and binding of HHLA2-mouse IgG2a was detected with 5 μg/ml Alexa647 conjugated 298.6F8 mAb (mouse antibody specific for mouse IgG2a mutated at L235E, E318A, K320A, K322A, generated in our lab). EC50 and IC50 analysis were conducted using Graph Pad Prism.

T-cell activation and culture

Ficoll density gradient (Ficoll-Paque PLUS; cat. #17144003) and RosetteSep Human T Cell Enrichment Cocktail (Stemcell; cat. #15021) were used according to the manufacturer's protocol to isolate T cells by negative selection from the blood of healthy donors. Donors signed a clinical consent form for the donation procedure which includes language that the donor center can direct use of all materials and byproducts for clinical or research use. T cells were activated using ImmunoCult Human CD3/CD28 T Cell Activator tetramers following the manufacturer's recommended protocol (Stemcell; cat. #10971) and cultured using ImmunoCult-XF T Cell Expansion Medium (Stemcell; cat. #10981) in the presence of 100U/ml of IL2 (Peprotech; cat. #200–02). At the indicated times, T cells were stained with the following antibodies: Alexa 647 conjugated 1G7 antibody (anti-KIR3DL3 antibody, generated as described in Methods) or Alexa 647 conjugated Mouse IgG2b, κ isotype control (Biolegend; cat. #400330) at 5μg/ml; BV785 anti-human CD3 (Biolegend; cat. #344842); PE/Cyanine7 conjugated anti-human CD8 (Biolegend; cat. #344712); PE/Cyanine7 conjugated anti-human CD4 (Biolgend; cat. #317414); PE/Cyanine7 conjugated Mouse IgG2b, κ isotype (Biolegend; cat. #400325); PE/Cyanine7 conjugated Mouse IgG1, κ isotype (Biolegend; cat. #400125); and BV785 conjugated Mouse IgG1, κ isotype (Biolegend; cat. #400169).

Reporter assays

TMIGD2_NFAT_Jurkat reporter activity: HHLA2- anti-CD3 scFV CHO (clone # 28) and anti-CD3 scFV -CHO cells were seeded at 2×10^4 cells/well density in CHOK1 growth medium as described above (see Cell lines and cell culture) in a white opaque bottom 96-well plate (Corning 3917) and incubated overnight at 37°C with 5% CO_2. The next day, medium was removed and cells were incubated with indicated HHLA2 antibody in 50 μl Jurkat cell medium for one hour at 37°C with 5% CO_2 before the addition of TMIGD2_NFAT_Jurkat reporter cell line (clone # 62) at $4–5 \times 10^4$ cells/well in 50 μl Jurkat cell medium. The culture was incubated for 3–6 hours. Luciferase signal was produced by adding 100 μl ONE-Step™ Luciferase Assay System (BPS Bioscience; cat. #60690),

according to manufacturer's protocol and luminescence measured in a Luminiskan luminometer (Life Sciences; N07087).

KIR3DL3_IL2_Jurkat reporter activity: HHLA2- anti-CD3 scFV (clone # 28) or anti-CD3 scFV -CHO cells were seeded at 2×10^4 cells/well density in CHOK1 growth medium in a white opaque bottom 96-well plate (Corning 3917) and incubated overnight at 37°C with 5% CO_2. The next day, the medium was removed and cells were incubated with HHLA2 or KIR3DL3 antibodies in 50 μl Jurkat cell medium for one hour before the addition of KIR3DL3_IL2_Jurkat reporter cell line (Clone # 2–12) at $4–5 \times 10^4$ cells/well in 50 μl Jurkat cell medium plus CD28 antibody (clone 9.3, BioXcell; cat. #BE0248) at a final concentration of 1 μg/mL in 100 μL assay mixture per well. Luciferase signal was produced by adding 100 μl ONE-Step™ Luciferase Assay System, according to manufacturer's protocol and luminescence measured in a Luminiskan luminometer.

NK-cell cytotoxicity assay

Two independent NK cytotoxicity methods were used: One was a beta-galactosidase based assay in which NK-92 MI cell cytotoxicity was determined using a KILR detection kit (Eurofins/Discoverx; cat. #97–0001M). Using the manufacturer's recommendations, the target cells, K562 cells were infected with KILR Retroparticles (KILR® Retroparticles for Adherent & Suspension Cells (G418), Eurofins/Discoverx; cat. #97–0006). Infected cells were selected in 500 μg/ml geneticin. NK-92 MI (effector) cells were co-cultured in a 96-well plate with 10^4 K562 target cells at effector-to-target (E:T) ratios of 1:1, 3:1 and 5:1 at 37°C for 4 h. Cell lysis was detected on a luminometer 1 h after adding 100 μl KILR detection reagent to the effector cells or target cells at room temperature. Where indicated, NK-92 MI (effector) cells were incubated with the indicated HHLA2 or KIR3DL3 blocking antibodies at 0.1, 1.0 and 10 μg/ml concentrations and appropriate isotype controls and co-cultured with K562 (target) cells at a fixed E:T ratio of 3:1 at 37°C for 4 h. The percentage specific lysis was calculated as follows:

Specific lysis (%) = [optical density (OD) experimental group – OD target cell natural release control] / (OD target cell maximum release control – OD target cell natural release control) × 100. Maximum release was measured after treatment with lysis agent provided by manufacturer.

The second NK-cell cytotoxicity assay used was a calcein based assay in which Raji and HHLA2 transfected Raji cells (both β2-microglobulin knockout) were stained with 1 μM calcein AM (BioLegend; cat. #425201) in PBS for 20 minutes at room temperature then washed twice with PBS and resuspended in RPMI1640 medium supplemented with 10% FBS, 1% Gluta-Max and 1% Penicillin/Streptomycin at 2×10^6/ml. 5×10^4 Raji target cells and NK-92 MI effector cells at 1:1, 2:1 and 3:1 E/T ratios were cultured either in the presence of the indicated HHLA2 or KIR3DL3 blocking antibodies or isotype controls (for 4 hours in round bottom 96 well plates at 37°C with 5% CO_2. Plates were then put on ice and analyzed by flow cytometry. Analysis was performed using FlowJo. Percent cell lysis was calculated as follows: % cytotoxicity = % calcein AM^+ target cells in the absence of effectors (100%) – % calcein AM^+ target cells in the presence of effectors (E/T ratio +1).

CD107 Degranulation assay

Raji β2-microglobulin knockout and HHLA2 transfected Raji β2-microglobulin knockout cells were co-cultured in RPMI1640 medium supplemented with 10% FBS, 1% Gluta-Max and 1% Penicillin/Streptomycin with NK-92 MI cells for 3 hours at E:T ratios of 1:1, 2:1 and 3:1 in round-bottom 96-well plates at 37°C with 5% CO_2. Anti-KIR3DL3 (1G7) and mouse IgG2b isotype control (Bxcell; cat. #BE0086) were used at 10μg/ml. BV421 anti-human CD107a (Biolegend; cat. #328625), APC anti-human CD56 (Biolegend; cat. #362503), APC Mouse IgG1, κ Isotype control (Biolegend; cat. #400121) and BV421 Mouse IgG1, κ Isotype control (Biolegend; cat. #400157) were used at 1:100 dilution. Monensin Solution (1,000X) (Biolegend; cat 420701) was used at 1:1000 dilution and Cell Stimulation Cocktail, PMA/Ionomycin (Biolgend; cat. #423301) was used at 1:500 dilution. Subsequently the plate was put on ice and cells were analyzed for CD107a expression on CD56 gated cells using flow cytometry and FlowJo software.

Patient samples and approvals

All patient samples were collected on institutional review board (IRB) approved protocols at Beth Israel Deaconess Medical Center (BIDMC) or Dana-Farber Cancer Institute (DFCI), or through the IRB approved phase II clinical trial BMS-010 (NCT01354431). The patients with mRCC treated on IRB approved protocols (n=26) comprised the pilot cohort, 12 were treated at BIDMC and 14 at DFCI. All had received 1 or more (mean, median=2.5, 2; respectively) prior lines of therapy. Eleven of the patients in the DFCI cohort received nivolumab and 3 atezolizumab. Patients in the BIDMC cohort were noted to have received PD1 therapies.

The BMS-010 trial enrolled 168 patients who received 3 different doses of nivolumab. Ninety-eight patients had tissue samples available for correlative analysis and 69 of these patients had evaluable expression data for both HHLA2 and PDL1.

Immunohistochemistry (IHC) and scoring

Analysis of HHLA2 expression was performed by IHC using a mouse monoclonal HHLA2 antibody (clone 499.8D2; generated as described above in Antibody generation). The assay was validated using formalin-fixed, paraffin-embedded (FFPE) cell line controls demonstrated to be either positive or negative for HHLA2 expression by flow cytometry (Supplemental figure S1). Briefly, rehydrated paraffin embedded tissue sections were boiled in EDTA buffer pH 8 (Thermo Fisher) with a pressure cooker (Biocare Medical) for 30 seconds at 125°C. After cooling to room temperature (RT), tissue sections were successively incubated with a peroxidase block (Dual Endogenous Enzyme Block, Agilent) and a protein block (Serum Free Block, Agilent) for 10 minutes each. Sections were next incubated for 1 hour at RT with the primary HHLA2 antibody diluted in Antibody Diluent with Background Reducing Components (Agilent) (1:100 dilution). Tissue sections were then incubated for 30 minutes at RT with EnVision horseradish peroxidase (HRP)-conjugated goat anti-mouse IgG antibody (Agilent). Between steps, tissue sections were washed for 5 minutes in washing buffer (0.1 mM Tris, pH7.4 + 0.05% Tween 20). HRP activity was then visualized by the formation of a brown precipitate by applying 3,3-diaminobenzidine + substrate (DAB+, Agilent) for 5 minutes. Nuclei were counterstained with hematoxylin.

PDL1 IHC was performed on tissue specimens from the pilot cohort using a validated PDL1-specific mouse monoclonal antibody (clone 405.9A11, generated in our laboratory, available from Cell Signaling Technology; cat. #29122), as previously described (20–23). Tissue specimens from the CheckMate-010 trial had been previously analyzed for PDL1 expression by IHC using a verified assay developed by Dako (clone 28–8) (24).

Membranous HHLA2 and PDL1 expression were independently scored as percentage of positive tumor cells by S.S. and J-C.P. Interscorer discrepancies were resolved by consensus review.

Western blot analysis

Jurkat parental cells, Jurkat cells transfected with KIR3DL3, NK-92 cells and NK-92-MI cells were used to prepare protein lysates. Lysates were prepared with RIPA buffer with protease inhibitor cocktail per manufacturer's instructions (Thermo Fisher; complete Ultra tablets, mini, EDTA-free, Roche). Lysates were loaded into a single wide lane 4–15% gradient mini-Protean TGX gel (Biorad) and transferred by a semidry electroblotting method. Membranes were blocked with 12% non-fat milk and 1% normal goat serum in Tris-buffered saline with Tween20 (TBST) for 1 hour at RT. The membrane was washed with TBST and incubated with anti-KIR3DL3 (clone 574.1F12) at 5 μg/ml in TBST and 1% BSA at 4°C overnight in a multi-well-mini-blotter. Membranes were washed with TBST three times at RT and incubated with secondary antibody (1:4000, HRP-conjugated goat anti-mouse IgG, Santa Cruz; cat. #sc-2005) in TBST, 6% non-fat milk and 0.5% normal goat serum for 30 min. After 3 additional washes with TBST, a 1:1 ratio of ECL substrate: enhancer was added to the membrane (SuperSignal West Pico Stable Peroxide Solution, Supersignal West Pico Luminol/Enhancer Solution, Thermo Fisher) and imaged on Hyblot CL autoradiography film (Denville Scientific).

RNA extraction and quantitative real-time PCR

Total RNA was extracted from cell pellets (0.5×10^6 to 1×10^6 cells per pellet) using Purelink RNA mini Kit (Thermo Fisher) as per the manufacturer's protocol. cDNA synthesis was performed with the High Capacity RNA-to-cDNA Kit (Applied Biosystems, Thermo Fisher) according to the manufacturer's recommendations. RT-PCR was performed in Applied Biosystems™ 7500 Real-Time PCR Systems machine using Power SYBR™ Green PCR Master Mix according to the manufacturer's recommendations. The cDNA template was estimated at ~5ng per reaction. Primers designed in the lab and ordered as DNA oligos from Thermo Fisher. The primers used are listed below:

18S: fw 5'-GTAACCCGTTGAACCCCATT-3'; 5'-CCATCCAATCGGTAGTAGCG-3'

KIR3DL3: fw 5'-AGAAGACGGGATGCCTGTC-3'; rv 5'-GTGAACTGCAACATCTGTAGGT-3'

HHLA2: fw 5'-TACAAAGGCAGTGACCATTTGG-3'; rv 5'-AGGTGTAAATTCCTTCGTCCAGA-3'

*PDL1 (*CD274): fw 5'-TGGCATTTGCTGAACGCATTT-3'; rv 5'-TGCAGCCAGGTCTAATTGTTTT-3'

18S was used as internal control for each sample. Relative mRNA levels were determined by the 2-ΔΔCT formula, and experiments were repeated three times.

Analysis of mRNA expression in ccRCC patients

TCGA RSEM RNASeqV2 data for TCGA ccRCC patients (534 tumor patients and 72 normal samples for all analyses) were downloaded from the TCGA GDAC http://gdac.broadinstitute.org/runs/stddata__2016_01_28/data/KIRC/20160128/gdac.broadinstitute.org_KIRC.Merge_rnaseqv2__illuminahiseq_rnaseqv2__unc_edu__Level_3__RSEM_genes__data.Level_3.2016012800.0.0.tar.gz). To derive Transcripts per Million (TPM), the "scaled_estimate" output value was multiplied by 10^6. These TPM values were transformed to log2(TPM+1) and tumor and normal expression was compared for each gene using a Wilcoxon rank sum test.

Single-cell RNA Sequencing analysis of KIR3DL3

Expression of KIR3DL3 was assessed in a publicly available data base (https://www.ebi.ac.uk/gxa/sc/experiments/E-MTAB-6678/results/tsne?geneId=ENSG00000242019&perplexity=50&colourBy=metadata&metadata=inferred_cell_type_-_authors_labels) in first trimester decidual placenta samples.

Cytometry

Cells were analyzed on a Gallios Flow Cytometer (Configuration: 488 nm, 561 nm, 405 nm, 355 nm, and 635 nm) or a BD Fortessa Flow Cytometer. Data were analyzed with FlowJo or with Kaluza Software. For each experiment, 10,000 to 20,000 cells were analyzed.

Statistics

Data were analyzed using GraphPad Prism Software 7, unless otherwise indicated. All data are represented as mean ± S.D. (error bars) except where stated otherwise (see Figure legends). Student's t test and two-way ANOVA were used as indicated in the legends (non-significant (ns), $P \geq 0.05$; *$P \leq 0.05$; **$P \leq 0.01$; ***$P \leq 0.001$; ****$P \leq 0.0001$).

Graphical presentation using scatter plots and Spearman's rank correlation coefficient was used to assess the relationship between HHLA2 and PDL1 expression in the pilot and BMS-010 cohorts. The expression values in the scatter plot were slightly jittered to clearly show datapoints, rugs (tick marks) were added to both x- and y-axes to show the concentration of HHLA2 and PDL1 expression values.

Results

Identification and characterization of KIR3DL3 as a receptor for HHLA2

To identify an inhibitory receptor for HHLA2, we performed a receptor screen using soluble human HHLA2-mIgG2a fusion protein (HHLA2-Ig) on a library of ~5500 cell surface receptors each expressed individually in HEK293 cells on glass slides. The screen identified

KIR3DL3 as a positive signal for HHLA2 binding (Figure 1A, Supplemental figure S2A). As expected, HHLA2-Ig also bound to TMIGD2 and the Fc receptor, FCGR2A but not to EGFR, PD1 or PDL1 (Figure 1A). KIR3DL3 is a member of the KIR family whose ligand has not, to our knowledge, yet been described. Other members of the KIR family were present in the 5,500 cDNA screen that identified only KIR3DL3 as a receptor for HHLA2, but to confirm the specificity, we individually tested HHLA2-Ig binding to KIR3DL3 and other members of the KIR family. HHLA2-Ig bound only to KIR3DL3 and not to other members of the KIR family (Figure 1A, Supplemental figure S2).

To confirm the HHLA2–KIR3DL3 and HHLA2–TMIGD2 interactions, we assayed the binding of HHLA2-Ig to cells expressing TMIGD2 and KIR3DL3. KIR3DL3 and TMIGD2 were stably overexpressed in the 300.19 mouse pre-B cell leukemic cell line and transfected cells were incubated with HHLA2-mIgG2a and analyzed by flow cytometry. We found a dose-dependent binding of HHLA2 to its two receptors, KIR3DL3 and TMIGD2 with very similar 50% maximal binding levels indicating similar binding affinities for these two receptors (Figure 1B, Supplemental figure S3A). There was no binding to untransfected 300.19 cells or to 300.19 cells transfected with HHLA2. Similar specific binding was observed with KIR3DL3 and TMIGD2 transiently transfected 293T cells (Supplemental figures S3B and S3C).

Characterization of HHLA2 and KIR3DL3 antibodies

To further understand the HHLA2–KIR3DL3 interaction, we generated a panel of KIR3DL3 and HHLA2 antibodies and characterized their binding to antigen and capacity to block HHLA2 binding to either KIR3DL3 or TMIGD2 (Figure 2 and Supplemental table S1). Dose-dependent binding of KIR3DL3 and HHLA2 antibodies was observed to KIR3DL3 and HHLA2 transfected 300.19 cells, respectively (Figure 2A and C). All HHLA2 antibodies except 6D10 showed high affinity binding to their antigen. Blocking and non-blocking antibodies were identified. HHLA2 antibodies 2G2 and 6F10 blocked the interaction of HHLA2 with both KIR3DL3 and TMIGD2, while 2C4 and 6D10 antibodies only blocked the HHLA2–KIR3DL3 interaction but not the HHLA2–TMIGD2 interaction (Figure 2D and 2E, Supplemental table S1). KIR3DL3 mAbs 1G7, 2F11, and 8F7 showed potent binding to KIR3DL3 in a dose-dependent manner (Figure 2A). 1G7 and 2F11 blocked the interaction of KIR3DL3 with HHLA2 while 8F7 only weakly blocked the interaction (Figure 2B and Supplemental table S1). All KIR3DL3 antibodies specifically bound to KIR3DL3 and not to any other KIR family members except the 2F11 antibody, which also showed weak binding to KIR2DL5A (Supplemental table S2).

KIR3DL3 expression on T cells and NK-92 MI cells

Previously published studies show that TMIGD2 is expressed on naïve T cells and NK cells and is downmodulated with activation. Some NK cell receptors such as NKG2A and KIR receptors can be expressed on $CD8^+$ cells (17, 18, 25). We assessed the expression of KIR3DL3 on T cells. T cells were purified from donor whole blood, activated with CD3/CD28 antibody tetramers and KIR3DL3 expression was determined in gated $CD3^+CD4^+$ and $CD3^+CD8^+$ T cells (Figure 3A). Minimal KIR3DL3 expression (0.26% of CD4+ cells and 0.39% of CD8+ cells) was noted at day 0 (unactivated) (Figure 3B) and there was an

increase in KIR3DL3 expression in both $CD4^+$ and $CD8^+$ cells on days 3 and 10 which peaked on day 21 post activation (6.60% of $CD4^+$ cells and 5.69% of $CD8^+$ cells) (Figure 3C).

We identified an NK cell line, NK-92 MI, which endogenously expresses KIR3DL3. NK-92 MI was derived from the original NK92 by transfection of an IL2 cDNA and overexpresses IL2, obviating the need for exogenous application of IL2. KIR3DL3 was expressed on a minority of parental NK-92 cells but highly expressed by NK-92 MI cells by flow cytometry, Western blot and RT-PCR (Figure 3D, Supplemental figure S4). In addition, KIR3DL3 expression has been reported on decidual NK cells and we confirmed this by analyzing single-cell RNA data in publicly accessible databases (Supplemental figure S5).

KIR3DL3 is an immunoinhibitory checkpoint receptor in T cells for HHLA2

The cytoplasmic domain of KIR3DL3 contains one ITIM motif and is predicted to have an immunoinhibitory function. To assess the function of the HHLA2–KIR3DL3 interaction, Jurkat T cells expressing KIR3DL3 and an IL2 promoter containing NFAT, AP1 and NFkB response elements driving a luciferase reporter gene were co-cultured with CHO cells stably expressing cell surface anti-CD3 scFV alone or in combination with HHLA2. Soluble anti-CD28 mAb was added to provide a strong costimulatory signal and the luciferase activity was assessed. As expected, a CD3 signal was necessary for T-cell activation and a CD28 costimulatory signal significantly increased IL2 reporter activity (Figure 4A). We observed that an HHLA2-mediated signal through KIR3DL3 resulted in a significant decrease of T-cell activation, as measured by IL2 reporter activity. These results indicate that KIR3DL3 is an inhibitory checkpoint receptor.

To assess the effect of TMIGD2 signaling following HHLA2 engagement and anti-CD3 mAb activation, we overexpressed TMIGD2 in Jurkat cells expressing the NFAT response element driving the luciferase reporter gene. When TMIGD2-transfected Jurkat cells were co-cultured with CHO cells stably expressing cell surface anti-CD3 scFV alone or in combination with HHLA2, we observed that HHLA2 increased T-cell activation over CD3 signaling alone (Supplemental figure S6), consistent with TMIGD2's reported co-stimulatory activity.

To assess the functional consequences of blocking the HHLA2–KIR3DL3 interaction, both receptor blocking and non-blocking HHLA2 and KIR3DL3 antibodies were evaluated in the KIR3DL3 Jurkat reporter gene assay. Consistent with their receptor-blocking activity, the blocking HHLA2 mAbs 2C4, 2G2 and 6F10 enhanced IL2 reporter activity whereas the weak blocker 6D10 did not (Figure 4B). Similarly, KIR3DL3 mAbs 1G7 and 2F11 enhanced IL2 reporter activity and T-cell activation consistent with their receptor-blocking activity whereas the weak blocker 8F7 did not (Figure 4C and Table S1). The 2F11 mAb showed higher fold induction of IL2 reporter activity compared with 1G7, although the binding avidity of 1G7 was higher.

The HHLA2–KIR3DL3 interaction inhibits NK-cell cytolytic activity

To assess the effects of the HHLA2–KIR3DL3 interaction on NK-cell cytotoxicity, we used the NK cell line, NK-92MI, which endogenously produces IL2 and expresses KIR3DL3

(Figure 3B). NK-92MI cells were incubated with K562 cells or K562 cells engineered to stably express HHLA2. NK-92 MI cells efficiently lysed K562 targets but were less effective at lysing K562 cells expressing HHLA2 at all E:T ratios (Figure 5A, Supplemental figure S7). To confirm that HHLA2 expression inhibits NK-cell cytotoxicity, Raji cells were first engineered to eliminate surface expression of MHC class I by CRISPR-mediated deletion of β_2-microglobulin (B2M) to render them good targets for NK cells. NK cells are activated by the absence of MHC class I on target cells, and we confirmed that Raji-B2M knockout cells were efficiently lysed by NK-92 MI cells. Raji-B2M knockout cells were engineered to express HHLA2 and Figure 5B shows that HHLA2 expression on Raji-B2M knockout cells inhibits cytotoxicity by NK-92 MI cells at all E:T ratios.

To assess the effects of HHLA2 or KIR3DL3 antibodies on HHLA2 mediated inhibition of NK-cell cytotoxicity, K562-HHLA2 cells were incubated with NK-92 MI cells at a fixed E:T ratio of 3:1 in the presence of increasing concentrations of KIR3DL3 antibodies, 1G7 and 2F11 (Figure 5C), or HHLA2 antibodies, 2G2 and 2C4 (Figure 5D). All antibodies tested enhanced NK-cell cytotoxicity in a dose-dependent manner compared with isotype controls. These results from the K562 model were confirmed in the HHLA2-Raji-B2M knockout model at various E:T ratios and a fixed concentration of antibody where KIR3DL3 blocking mAbs 1G7 and 2F11 enhanced NK-cell cytotoxicity compared with isotype controls (Figure 5E). Additionally, HHLA2 blocking antibodies 2C4 and 2G2 enhanced NK-cell cytotoxicity (Figure 5F). 8F7, a KIR3DL3 antibody, and 6D10, an HHLA2 antibody, which are weak blockers of the KIR3DL3–HHLA2 interaction, did not enhance cytotoxicity (Figure 5E and 5F).

To examine the role of KIR3DL3 in regulating NK-cell lytic activity, we performed a CD107a degranulation assay. As measured by CD107a expression on the NK-92 MI cell surface (degranulation), HHLA2 expression on the Raji B2M knockout cells inhibits NK-92 MI degranulation (Figure 5G) and blockade of KIR3DL3 with the 1G7 mAb leads to enhanced degranulation of these NK cells (Figure 5H).

HHLA2 is expressed in RCC tumors and is non-overlapping with PDL1 expression

Pan-cancer transcriptomic analyses have demonstrated that HHLA2 is expressed in multiple tumor types, with RCC showing highest levels of expression compared with normal tissue (10). In our analysis of mRNA expression of B7 family members in the TCGA, we found that HHLA2 was the most highly upregulated B7 family member in ccRCC compared with normal kidney tissue (Figure 6A). PDL1, PDL2, B7H3 and VISTA transcripts were only slightly higher in ccRCC compared with normal kidney and B7H4 transcript was markedly reduced in ccRCC. As expected, CD8 transcripts were upregulated in ccRCC compared with normal kidney, reflecting the high immune infiltrate in ccRCC. To further investigate HHLA2 expression at the protein level in human samples, we validated the use of an HHLA2 mAb, 8D2, for IHC in formalin-fixed paraffin-embedded cells including HHLA2 expressing HDLM2 Hodgkin lymphoma or the 300.19 cell line transfected with HHLA2 (Supplemental figure S7). We performed IHC to detect HHLA2 and PDL1 expression in a cohort of primary RCC nephrectomy specimens from 26 patients. Figure 6B shows a scatter plot of HHLA2 and PDL1 expression score. There was a negative association between PDL1

and HHLA2 expression. This finding was validated in pre-treatment specimens from a larger cohort of patients enrolled in BMS-010 (Figure 6C). The Spearman rank correlation of −0.57 (p=0.003) and −0.23 (p=0.053), for the pilot and BMS-010 cohorts, respectively, indicates a negative association between PDL1 and HHLA2 expression. Of note, not only did we find that HHLA2 and PDL1 expression were non-overlapping among patients but generally also within tumors. In tumors in which both molecules were present, PDL1 and HHLA2 were generally expressed in distinct, non-overlapping regions but in rare cases colocalized (Figure 6B, single red dot in upper right of figure). For example, Figure 6D and 6E illustrates a tumor where the region that expresses HHLA2 does not express PDL1 and conversely, the region that expresses PDL1 does not express HHLA2. To understand the potential mechanisms by which differential expression is regulated, we assessed whether HHLA2 expression is regulated by IFNγ, which has been shown to upregulate PD-L1 expression. We found that IFNγ treatment strongly induced PDL1 mRNA expression in RCC cell lines but HHLA2 mRNA expression was not affected by IFNγ exposure. HHLA2 levels were also not affected by TGFβ or IL10, other cytokines found in the tumor microenvironment (Figure 6F).

Discussion

HHLA2 is a B7 family member with both immune stimulatory and inhibitory functions (11–13, 15, 25). TMIGD2 has previously been characterized as the immune-stimulatory receptor for HHLA2 in both T cells and NK cells but the mechanisms by which HHLA2 could inhibit T cells and NK has been unknown (Figure 7). We hypothesized the presence of an inhibitory receptor that could mediate this effect (14). We performed a screen for HHLA2 receptors using soluble recombinant HHLA2-mIgG2a on an array of cell-surface receptors and identified KIR3DL3 as a receptor for HHLA2. KIR3DL3 is a member of the KIR family of receptors but to our knowledge its ligand was not known before now. We show that the HHLA2–KIR3DL3 interaction is immune inhibitory in T cells and NK cells and that antibodies that block this interaction reverse the immune inhibition. IHC analysis for HHLA2 expression in RCC patient tumors showed a largely non-overlapping pattern of expression with PDL1. Taken together, these findings suggest blockade of the KIR3DL3–HHLA2 interaction could represent a novel approach for cancer immunotherapy.

Members of the KIR family contribute to both innate and adaptive immune responses through their expression by NK cells and T cells (16–19). HLA class I ligands have been identified for 9 of the 13 KIR but no HLA ligand for KIR3DL3 has been identified (16). The KIRs have a similar protein structure with 2 or 3 extracellular Ig domains and either a short (activating DS form) or long intracellular domain (inhibiting DL form) containing ITIMs. The KIR3DL3 gene encodes three extracellular Ig domains, has only one ITIM and lacks the exon encoding the stem between the Ig domains and the transmembrane region. Although the structure of KIR3DL3 is suggestive of an inhibitory receptor, to our knowledge, before our study, the function of KIR3DL3 was not known and cognate ligands had not been identified.

The expression of individual KIR genes is clonally distributed with only a fraction of NK cells and T cells expressing a given KIR repertoire. In individuals, the 13 KIR genes vary in

their presence and copy number but KIR3DL3 is unique in the KIR family as it is present in all individuals (16). The KIR3DL3 promoter is the strongest of the KIR promoters but is generally silenced by methylation (27). KIR3DL3 is highly polymorphic; however, the majority of the 157 polymorphic residues map to sites distinct from known HLA ligand binding sites of other KIRs based on a KIR3DL3 structure model (21,28). This suggests these polymorphisms are unlikely to affect HHLA2 ligand binding. Future studies mapping KIR3DL3 ligand-binding sites will elucidate the effect of KIR3DL3 polymorphisms on HHLA2 ligand binding and NK cell and T cell activation.

KIR3DL3 is rarely expressed in normal tissues except for placental decidual NK cells and activated NK cells (29). HHLA2 is highly expressed on placental trophoblasts (8). This expression pattern is similar to PDL1 expression on placental trophoblasts and other sites of immune privilege and consistent with a primary natural role in immune suppression (30). In our study, we identify HHLA2 as a ligand for KIR3DL3 and show its function as an inhibitory receptor in NK cells and T cells.

Consistent with our observation that the HHLA2–KIR3DL3 interaction inhibits CD28-dependent CD3 signaling in T cells, Reider, et al. also showed that HHLA2-Fc inhibits T-cell activation mediated by CD3 and CD28 signaling and ERK2 tyrosine phosphorylation (20). These observations are similar to results showing PDL1–PD1 interaction inhibits a CD3 signaling pathway dependent on tyrosine phosphorylation and MEK1–ERK2 activation (31,32). Inhibition of CD3 signaling by PDL1 is through tyrosine phosphorylation of the PD1 immunoreceptor tyrosine-based switching motif (ITSM) and recruitment of SHP2 phosphatase, which dephosphorylates proximal signaling molecules of the TCR and CD28 pathways (33–36). Taken together, the above results suggest that PD1 and KIR3DL3 may share similar pathways following T-cell activation and inhibition of both pathways could be additive.

Expression of inhibitory immune receptors on T cells is dynamically modulated with activation. The HHLA2–KIR3DL3 pathway has parallels to the B7–CTLA-4 pathway. Resting T cells express immune stimulatory receptors such as CD28 (for CD80/86) (37–39) and TMIGD2 (for HHLA2) (7, 11). TMIGD2 is primarily expressed on naive T cells and is downmodulated upon T-cell activation and only expressed on 22% of memory $CD4^+$ T cells and 29% of memory $CD8^+$ T cells. (7,11,37,38). Similarly, CD28 is expressed on only 50% of antigen-experienced human $CD8^+$ T cells (39). Upon activation, T cells upregulate expression of inhibitory receptors including CTLA-4, PD-1, and KIR3DL3 ((40–41) and our data). We show that KIR3DL3 expression is rare in non-activated T cells and is induced in a modest subpopulation of $CD4^+$ and $CD8^+$ T cells following stimulation with anti-CD3 and CD28 mAbs. Unlike the early PD1 expression following T-cell activation, KIR3DL3 is expressed later and peaks around day 21 following T-cell activation. This pattern of regulation predicts that neoantigen-experienced T cells will express a preponderance of immunoinhibitory receptors at different times following activation. If the cognate ligands (B7 or HHLA2) are present, T cell inhibition can become the dominant outcome.

RCC is a malignancy with many recent therapeutic advances. It is highly immune infiltrated and has historically been immune responsive. IL2 therapy has been an immunotherapy

option for patients since 1992 (42,43). More recently, inhibitors of the PD1 pathway have not only shown activity as monotherapy but are also approved in combination with VEGFR tyrosine kinase inhibitor therapy or CTLA4-targeted immunotherapy (45–47). However, resistance to therapy is seen in many patients and new treatment options are needed.

We have shown that HHLA2 expression and PDL1 expression are non-overlapping in RCC. This is consistent with a prior report on non-small cell lung cancer (NSCLC) in which 64% of tumor samples were HHLA2 positive. and of these, 67% were PDL1 negative (47). This study in NSCLC together with our HHLA2 and PDL1 expression studies in ccRCC provide a rationale for targeting the HHLA2–KIR3DL3 immune checkpoint pathway alone or in combination with PD1 inhibitors in these cancers and other cancers where the HHLA2 inhibitory pathway has been implicated.

In this study, we have identified KIR3DL3 as the inhibitory receptor for HHLA2 and generated checkpoint inhibitor antibodies that reverse HHLA2–KIR3DL3-mediated inhibition in T cells and NK cells. Most of the HHLA2 antibodies generated block binding of HHLA2 to both TIMGD2 and KIR3DL3. Antibodies that block only one of these two receptor interactions were rare. Thus, the HHLA2 binding sites on TMIGD2 and KIR3DL3 appear to be overlapping but non-identical. We found that HHLA2 antibodies that block the KIR3DL3–HHLA2 interaction but preserve the TMIGD2 stimulatory signal may be one option for therapeutic development. Additionally, KIR3DL3 antibodies that selectively block KIR3DL3–HHLA2 interactions are also attractive candidates for further development.

Many immune combinations have been tested in preclinical models and multiple candidates have progressed to clinical trials. Most have not yet shown outstanding clinical activity. One hypothesis for this limited efficacy is that many pathways being co-targeted with PDL1 share mechanisms for upregulation of expression. For example, indoleamine 2,3-dioxygenase (IDO) inhibition in cancer has been of interest but clinical trials of IDO and PD1 combinations have not yielded promising results (48). IFNγ upregulates both IDO and PDL1 expression. We show that HHLA2 expression is not regulated by IFNγ and thus may represent an independently regulated mechanism of tumor immune evasion. Additionally, HHLA2 immune signaling is important not only in T cells but in NK cells and inhibition of HHLA2 signaling through KIR3DL3 may affect a diverse set of lymphocytes in the immune microenvironment that mediate both innate and adaptive immune responses. In tumors, HHLA2 and PDL1 expression appear to be non-overlapping and independently regulated. We are currently studying pathways that upregulate HHLA2 expression.

Both the receptors and ligands of the HHLA2–KIR3DL3/TMIGD2 pathway are expressed in primates and not found in multiple other mammals including rodents, which is unique within the B7 and CD28 families. Thus, our functional studies of this pathway are limited to *in vitro* models using human cell lines and primary immune cells. To assess the *in vivo* role of this pathway, humanized models need to be developed. A triple knock-in approach would be needed including genomic regulatory regions and complete genes as both the receptors and ligand have no murine orthologs. It is possible that this limitation may indicate that HHLA2 is part of a more multi-layered and non-redundant immune response not needed in short-

lived rodent species. This suggests that transplantable mouse tumor models cannot accurately predict all immune therapeutic activity in humans.

Another limitation is the low expression of KIR3DL3. The NK-92 MI cell line expresses KIR3DL3 in contrast to the parental NK92 cell line. IL2 likely plays a role in the regulation of KIR3DL3 and we are currently exploring this hypothesis. It is likely that KIR3DL3 is dynamically regulated during the anti-tumor immune response and that blockade of KIR3DL3 in a subpopulation of the immune microenvironment would be amplified to achieve stimulatory effects on the anti-tumor immune response.

Immune checkpoint inhibition of the PD1 pathway is now the cornerstone for immune therapy of cancer. Despite the success of PD1 inhibition, many patients develop resistance and identification of novel, non-redundant, immune inhibitory pathways is an important need in this field. Shifting the balance of immune inhibitory and stimulatory pathways away from inhibition may optimize the anti-tumor immune response. In summary, we identify KIR3DL3 as an immune inhibitory receptor for HHLA2. We have identified HHLA2 and KIR3DL3 antibodies that specifically block the immune inhibitory activity but spare the co-stimulatory activity of TMIGD2 (Figure 7). Phase I clinical trials testing the safety and preliminary efficacy of HHLA2 pathway inhibition are currently being developed.

Supplementary Material

Refer to Web version on PubMed Central for supplementary material.

Funding information:

This work was supported by NIH R01 CA196996 (RSB), NIH P50 CA101942-12 (RSB, KMM, PJC, SS, GJF), P50CA206963 (GJF), and AI056299 (GJF), Advanced Discovery Award (2019-1517) from the Kidney Cancer Association (KM, RB, GF). The U.S. Army Medical Research Acquisition Activity, 820 Chandler Street, Fort Detrick MD 21702-5014 is an awarding and administering acquisition office. This work was supported by the Department of Defense (DOD), through a KCRP Concept Award (KC170139). Opinions, interpretations, conclusions and recommendations are those of the author and are not necessarily endorsed by the DOD. Study samples from BMS-010 were shared by Bristol Myers Squibb.

References

1. Zou W, Wolchok JD, Chen L. PD-L1 (B7-H1) and PD-1 pathway blockade for cancer therapy: Mechanisms, response biomarkers, and combinations. Sci Transl Med. 2016;8(328):328rv4.
2. Baumeister SH, Freeman GJ, Dranoff G, Sharpe AH. Coinhibitory Pathways in Immunotherapy for Cancer. Annu Rev Immunol. 2016;34:539–73. [PubMed: 26927206]
3. Sharma P, Allison JP. The future of immune checkpoint therapy. Science. 2015;348(6230):56–61. [PubMed: 25838373]
4. Pitt JM, Vetizou M, Daillere R, Roberti MP, Yamazaki T, Routy B, et al. Resistance Mechanisms to Immune-Checkpoint Blockade in Cancer: Tumor-Intrinsic and -Extrinsic Factors. Immunity. 2016;44(6):1255–69. [PubMed: 27332730]
5. Zaretsky JM, Garcia-Diaz A, Shin DS, Escuin-Ordinas H, Hugo W, Hu-Lieskovan S, et al. Mutations Associated with Acquired Resistance to PD-1 Blockade in Melanoma. N Engl J Med. 2016;375(9):819–29. [PubMed: 27433843]
6. O'Donnell JS, Long GV, Scolyer RA, Teng MW, Smyth MJ. Resistance to PD1/PDL1 checkpoint inhibition. Cancer Treat Rev. 2017;52:71–81. [PubMed: 27951441]

7. Crespo J, Vatan L, Maj T, Liu R, Kryczek I, Zou W. Phenotype and tissue distribution of CD28H(+) immune cell subsets. Oncoimmunology. 2017;6(12):e1362529. [PubMed: 29209568]
8. Janakiram M, Chinai JM, Fineberg S, Fiser A, Montagna C, Medavarapu R, et al. Expression, Clinical Significance, and Receptor Identification of the Newest B7 Family Member HHLA2 Protein. Clin Cancer Res. 2015;21(10):2359–66. [PubMed: 25549724]
9. Zhou QH, Li KW, Chen X, He HX, Peng SM, Peng SR, et al. HHLA2 and PD-L1 co-expression predicts poor prognosis in patients with clear cell renal cell carcinoma. J Immunother Cancer. 2020;8(1).
10. Wang B, Ran Z, Liu M, Ou Y. Prognostic Significance of Potential Immune Checkpoint Member HHLA2 in Human Tumors: A Comprehensive Analysis. Front Immunol. 2019;10:1573. [PubMed: 31379814]
11. Zhu Y, Yao S, Iliopoulou BP, Han X, Augustine MM, Xu H, et al. B7-H5 costimulates human T cells via CD28H. Nat Commun. 2013;4:2043. [PubMed: 23784006]
12. Zhao R, Chinai JM, Buhl S, Scandiuzzi L, Ray A, Jeon H, et al. HHLA2 is a member of the B7 family and inhibits human CD4 and CD8 T-cell function. Proc Natl Acad Sci U S A. 2013;110(24):9879–84. [PubMed: 23716685]
13. Wang J, Manick B, Wu G, Hao R. Biofunctions of three new B7 family members (IRM7P.486). J Immunol. 2014;192((1 Supplement)):126.11.
14. Xiao Y, Freeman GJ. A New B7:CD28 Family Checkpoint Target for Cancer Immunotherapy: HHLA2. Clin Cancer Res. 2015;21(10):2201–3. [PubMed: 25869386]
15. Zhuang X, Long EO. CD28 Homolog Is a Strong Activator of Natural Killer Cells for Lysis of B7H7(+) Tumor Cells. Cancer Immunol Res. 2019;7(6):939–51. [PubMed: 31018957]
16. Pende D, Falco M, Vitale M, Cantoni C, Vitale C, Munari E, et al. Killer Ig-Like Receptors (KIRs): Their Role in NK Cell Modulation and Developments Leading to Their Clinical Exploitation. Front Immunol. 2019;10:1179. [PubMed: 31231370]
17. Bakker AB, Phillips JH, Figdor CG, Lanier LL. Killer cell inhibitory receptors for MHC class I molecules regulate lysis of melanoma cells mediated by NK cells, gamma delta T cells, and antigen-specific CTL. J Immunol. 1998;160(11):5239–45. [PubMed: 9605119]
18. Guerra N, Guillard M, Angevin E, Echchakir H, Escudier B, Moretta A, et al. Killer inhibitory receptor (CD158b) modulates the lytic activity of tumor-specific T lymphocytes infiltrating renal cell carcinomas. Blood. 2000;95(9):2883–9. [PubMed: 10779435]
19. Leaton LA, Shortt J, Kichula KM, Tao S, Nemat-Gorgani N, Mentzer AJ, et al. Conservation, Extensive Heterozygosity, and Convergence of Signaling Potential All Indicate a Critical Role for KIR3DL3 in Higher Primates. Front Immunol. 2019;10:24. [PubMed: 30745901]
20. Gaule P, Smithy JW, Toki M, Rehman J, Patell-Socha F, Cougot D, et al. A Quantitative Comparison of Antibodies to Programmed Cell Death 1 Ligand 1. JAMA Oncol. 2017;3(2):256–9. [PubMed: 27541827]
21. Mahoney KM, Sun H, Liao X, Hua P, Callea M, Greenfield EA, et al. PD-L1 Antibodies to Its Cytoplasmic Domain Most Clearly Delineate Cell Membranes in Immunohistochemical Staining of Tumor Cells. Cancer Immunol Res. 2015;3(12):1308–15. [PubMed: 26546452]
22. Callea M, Albiges L, Gupta M, Cheng SC, Genega EM, Fay AP, et al. Differential Expression of PD-L1 between Primary and Metastatic Sites in Clear-Cell Renal Cell Carcinoma. Cancer Immunol Res. 2015;3(10):1158–64. [PubMed: 26014095]
23. Perez JA, Goldsack E, Norambuena L. [Medullary carcinoma of the thyroid. Clinical case]. Rev Med Chil. 1989;117(4):431–4. [PubMed: 2519398]
24. Pignon JC, Jegede O, Shukla SA, Braun DA, Horak CE, Wind-Rotolo M, et al. irRECIST for the Evaluation of Candidate Biomarkers of Response to Nivolumab in Metastatic Clear Cell Renal Cell Carcinoma: Analysis of a Phase II Prospective Clinical Trial. Clin Cancer Res. 2019;25(7):2174–84. [PubMed: 30670497]
25. Mingari MC, Schiavetti F, Ponte M, Vitale C, Maggi E, Romagnani S, et al. Human CD8+ T lymphocyte subsets that express HLA class I-specific inhibitory receptors represent oligoclonally or monoclonally expanded cell populations. Proc Natl Acad Sci U S A. 1996;93(22):12433–8. [PubMed: 8901599]

26. Rieder SA, Wang J, White N, Qadri A, Menard C, Stephens G, et al. B7-H7 (HHLA2) inhibits T-cell activation and proliferation in the presence of TCR and CD28 signaling. Cell Mol Immunol. 2020.
27. Trompeter HI, Gomez-Lozano N, Santourlidis S, Eisermann B, Wernet P, Vilches C, et al. Three structurally and functionally divergent kinds of promoters regulate expression of clonally distributed killer cell Ig-like receptors (KIR), of KIR2DL4, and of KIR3DL3. J Immunol. 2005;174(7):4135–43. [PubMed: 15778373]
28. Vivian JP, Duncan RC, Berry R, O'Connor GM, Reid HH, Beddoe T, et al. Killer cell immunoglobulin-like receptor 3DL1-mediated recognition of human leukocyte antigen B. Nature. 2011;479(7373):401–5. [PubMed: 22020283]
29. Trundley AE, Hiby SE, Chang C, Sharkey AM, Santourlidis S, Uhrberg M, et al. Molecular characterization of KIR3DL3. Immunogenetics. 2006;57(12):904–16. [PubMed: 16391939]
30. Brown JA, Dorfman DM, Ma FR, Sullivan EL, Munoz O, Wood CR, et al. Blockade of programmed death-1 ligands on dendritic cells enhances T cell activation and cytokine production. J Immunol. 2003;170(3):1257–66. [PubMed: 12538684]
31. Sheppard KA, Fitz LJ, Lee JM, Benander C, George JA, Wooters J, et al. PD-1 inhibits T-cell receptor induced phosphorylation of the ZAP70/CD3zeta signalosome and downstream signaling to PKCtheta. FEBS Lett. 2004;574(1–3):37–41. [PubMed: 15358536]
32. Chemnitz JM, Parry RV, Nichols KE, June CH, Riley JL. SHP-1 and SHP-2 associate with immunoreceptor tyrosine-based switch motif of programmed death 1 upon primary human T cell stimulation, but only receptor ligation prevents T cell activation. J Immunol. 2004;173(2):945–54. [PubMed: 15240681]
33. Hui E, Cheung J, Zhu J, Su X, Taylor MJ, Wallweber HA, et al. T cell costimulatory receptor CD28 is a primary target for PD-1-mediated inhibition. Science. 2017;355(6332):1428–33. [PubMed: 28280247]
34. Patsoukis N, Duke-Cohan JS, Chaudhri A, Aksoylar HI, Wang Q, Council A, et al. Interaction of SHP-2 SH2 domains with PD-1 ITSM induces PD-1 dimerization and SHP-2 activation. Commun Biol. 2020;3(1):128. [PubMed: 32184441]
35. Boussiotis VA. Molecular and Biochemical Aspects of the PD-1 Checkpoint Pathway. N Engl J Med. 2016;375(18):1767–78. [PubMed: 27806234]
36. Sharpe AH, Freeman GJ. The B7-CD28 superfamily. Nat Rev Immunol. 2002;2(2):116–26. [PubMed: 11910893]
37. Tian Y, Sun Y, Gao F, Koenig MR, Sunderland A, Fujiwara Y, et al. CD28H expression identifies resident memory CD8 + T cells with less cytotoxicity in human peripheral tissues and cancers. Oncoimmunology. 2019;8(2):e1538440. [PubMed: 30713797]
38. Zhong C, Lang Q, Yu J, Wu S, Xu F, Tian Y. Phenotypical and potential functional characteristics of different immune cells expressing CD28H/B7-H5 and their relationship with cancer prognosis. Clin Exp Immunol. 2020;200(1):12–21. [PubMed: 31901178]
39. Lum LG, Orcutt-Thordarson N, Seigneuret MC, Hansen JA. In vitro regulation of immunoglobulin synthesis by T-cell subpopulations defined by a new human T-cell antigen (9.3). Cell Immunol. 1982;72(1):122–9. [PubMed: 6216957]
40. Linsley PS, Greene JL, Tan P, Bradshaw J, Ledbetter JA, Anasetti C, et al. Coexpression and functional cooperation of CTLA-4 and CD28 on activated T lymphocytes. J Exp Med. 1992;176(6):1595–604. [PubMed: 1334116]
41. Agata Y, Kawasaki A, Nishimura H, Ishida Y, Tsubata T, Yagita H, et al. Expression of the PD-1 antigen on the surface of stimulated mouse T and B lymphocytes. Int Immunol. 1996;8(5):765–72. [PubMed: 8671665]
42. Margolin KA, Rayner AA, Hawkins MJ, Atkins MB, Dutcher JP, Fisher RI, et al. Interleukin-2 and lymphokine-activated killer cell therapy of solid tumors: analysis of toxicity and management guidelines. J Clin Oncol. 1989;7(4):486–98. [PubMed: 2647914]
43. Atkins MB, Lotze MT, Dutcher JP, Fisher RI, Weiss G, Margolin K, et al. High-dose recombinant interleukin 2 therapy for patients with metastatic melanoma: analysis of 270 patients treated between 1985 and 1993. J Clin Oncol. 1999;17(7):2105–16. [PubMed: 10561265]

44. Motzer RJ, Penkov K, Haanen J, Rini B, Albiges L, Campbell MT, et al. Avelumab plus Axitinib versus Sunitinib for Advanced Renal-Cell Carcinoma. N Engl J Med. 2019;380(12):1103–15. [PubMed: 30779531]

45. Rini BI, Plimack ER, Stus V, Gafanov R, Hawkins R, Nosov D, et al. Pembrolizumab plus Axitinib versus Sunitinib for Advanced Renal-Cell Carcinoma. N Engl J Med. 2019;380(12):1116–27. [PubMed: 30779529]

46. Motzer RJ, Tannir NM, McDermott DF, Aren Frontera O, Melichar B, Choueiri TK, et al. Nivolumab plus Ipilimumab versus Sunitinib in Advanced Renal-Cell Carcinoma. N Engl J Med. 2018;378(14):1277–90. [PubMed: 29562145]

47. Cheng H, Borczuk A, Janakiram M, Ren X, Lin J, Assal A, et al. Wide Expression and Significance of Alternative Immune Checkpoint Molecules, B7x and HHLA2, in PD-L1-Negative Human Lung Cancers. Clin Cancer Res. 2018;24(8):1954–64. [PubMed: 29374053]

48. Munn DH. Blocking IDO activity to enhance anti-tumor immunity. Front Biosci (Elite Ed). 2012;4:734–45. [PubMed: 22201909]

Synopsis:

The B7 family member HHLA2 delivers costimulatory signals via TMIGD2. The data show KIR3DL3 is an inhibitory receptor for HHLA2 and that HHLA2 is expressed in kidney cancer separately from PDL1; targeting this interaction could be immunotherapeutic.

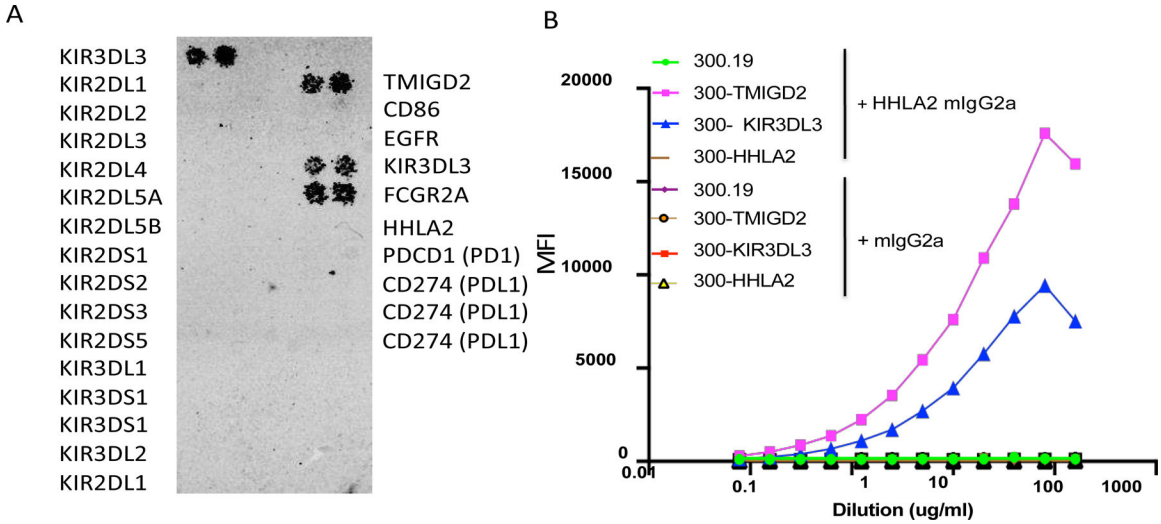

Figure 1: Expression screen identifying KIR3DL3 as a receptor for HHLA2.

(**A**) Cell microarray analysis using soluble HHLA2–mIgG2a (HHLA2-Ig) to bind the indicated cell-surface receptors individually expressed in HEK293 cells. HHLA2-Ig bound to TMIGD2, KIR3DL3, and control (FCGR2A) but not to other members of the KIR family, PD-1, PD-L1 or HHLA2. This screen was performed in duplicate plates. (**B**) Flow cytometric analysis of HHLA2-Ig or control Ig binding to control 300.19 cells or 300.19 cells stably expressing KIR3DL3, TMIGD2, or HHLA2 using the indicated concentrations of HHLA2-Ig or isotype control (from 0.1 μg/mL to 160 μg/mL). (n≥3 replicates)

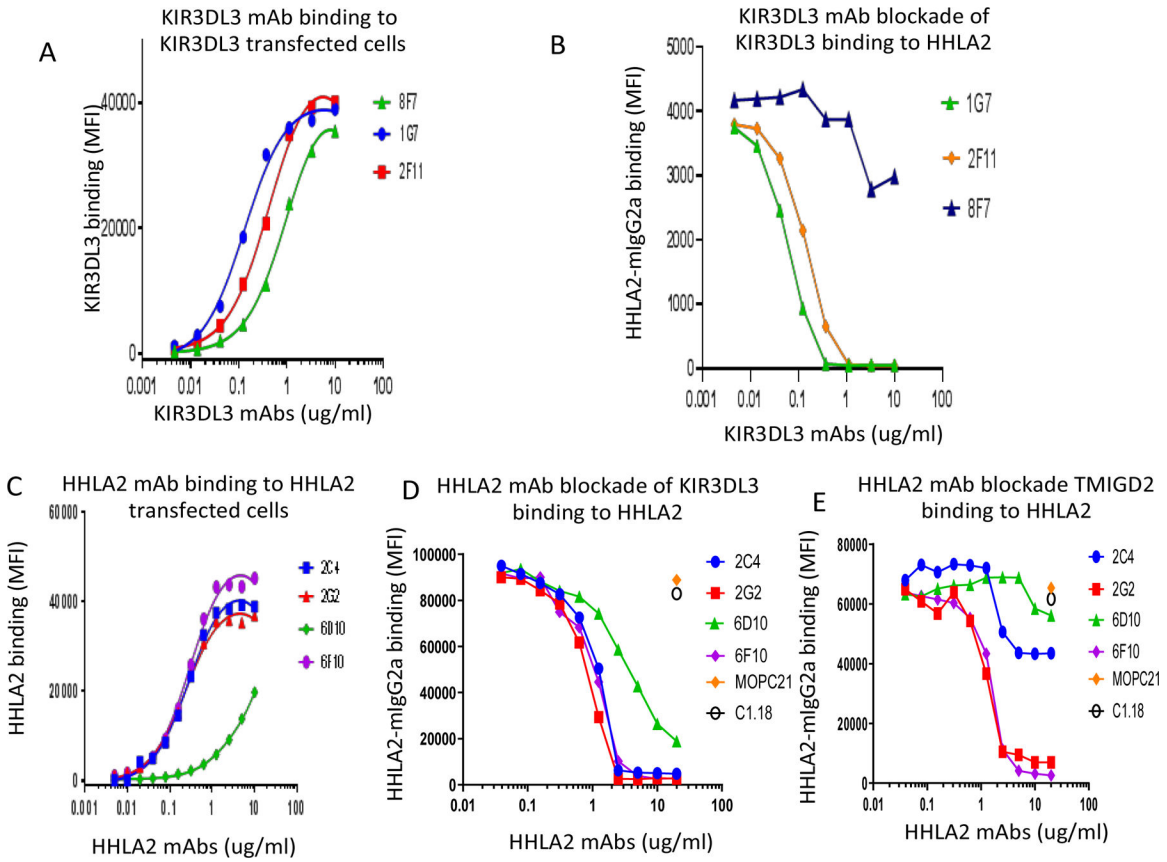

Figure 2: Characterization of a panel of KIR3DL3 and HHLA2 mAbs.

Flow cytometric analysis of binding of (**A**) KIR3DL3 mAbs to 300.19 cells expressing KIR3DL3. (**B**) Capacity of KIR3DL3 mAbs to block binding of HHLA2-Ig to 300.19 cells expressing KIR3DL3. (**C**) HHLA2 mAbs bind to 300.19 cells expressing HHLA2 with 2C4, 2G2 and 6F10 showing strongest binding and less with 6D10. (**D**) Capacity of HHLA2 mAbs to block binding of HHLA2-Ig to 300.19 cells expressing KIR3DL3 with 2C4, 2G2 and 6F10 showing strongest binding. (**E**) Capacity of HHLA2 mAbs 2G2 and 6F10 to block binding of HHLA2-Ig to 300.19 cells expressing TMIGD2. Representative binding experiments are shown: n≥3 replicates.

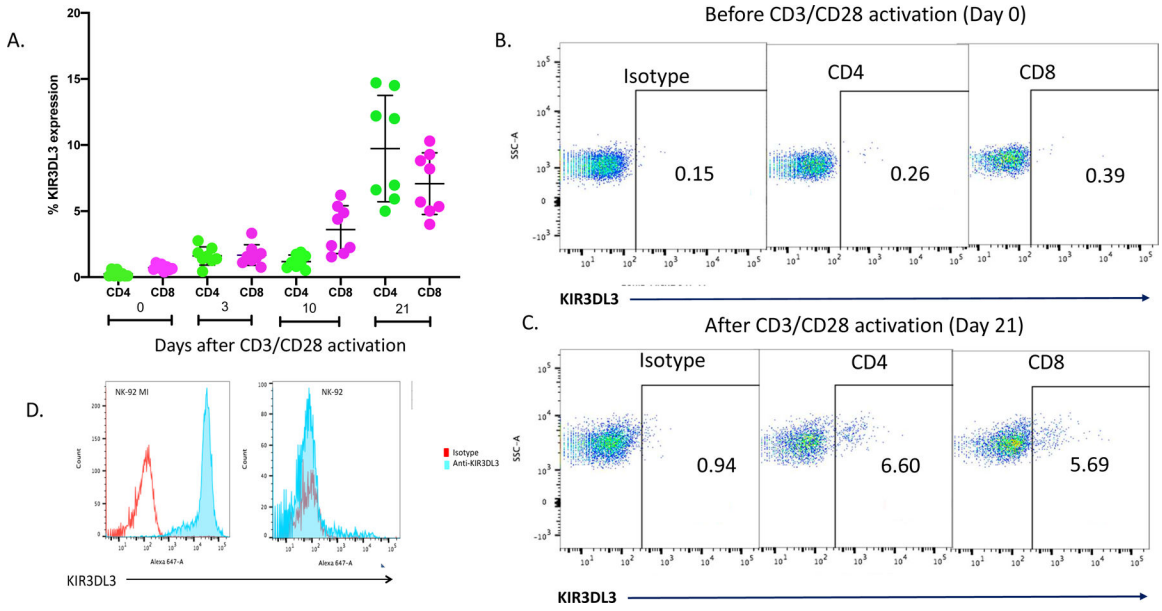

Figure 3: KIR3DL3 expression on activated human T cells and NK-92 MI cells.

(A) T cells were purified from whole blood of 4 normal donors and activated with CD3/CD28 antibody tetramers and flow cytometric analysis was performed in duplicate at the indicated days to assess KIR3DL3 expression in gated $CD3^+CD4^+$ and $CD3^+CD8^+$ T cells. Plots show all values measured with the center of the whiskers plot representing the median. Representative plots showing KIR3DL3 expression at (**B**) day 0 (unactivated) and (**C**) day 21 post activation. N=2 experiments with similar results. (**D**) KIR3DL3 expression on NK-92 MI (left panel) but minimally on NK-92 cells (right panel). N>3 replicates.

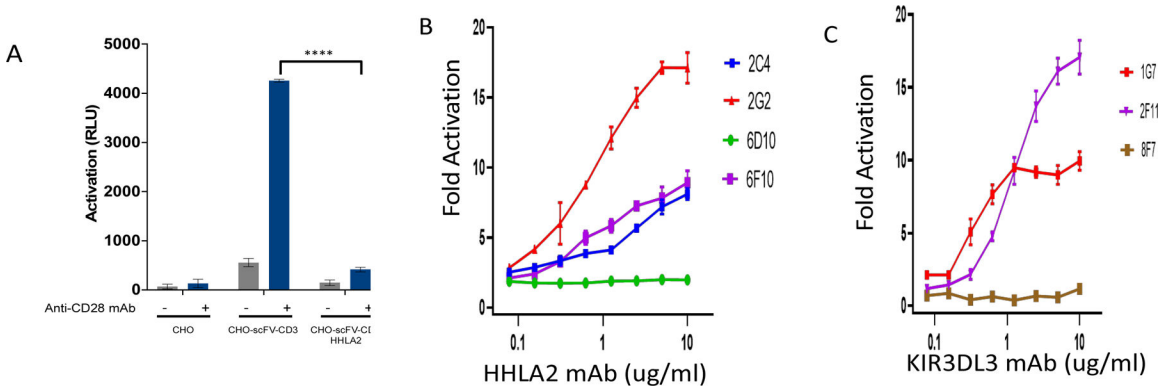

Figure 4: KIR3DL3 is an inhibitory receptor in T cells and T-cell activation is enhanced by HHLA2/KIR3DL3 blockade.

(**A**) Jurkat IL2-reporter T cells expressing KIR3DL3 were co-cultured with CHO cells expressing anti-CD3 scFV, CHO cells coexpressing anti-CD3 scFV and HHLA2, or untransfected CHO cells in the presence or absence of CD28 mAb as indicated. Luciferase activity represented as relative light units (RLU). (**B, C**) Jurkat IL2-reporter T cells expressing KIR3DL3 were co-cultured with CHO cells coexpressing anti-CD3 scFV and HHLA2 in the presence of CD28 mAb and (**B**) HHLA2 mAbs or (**C**) KIR3DL3 mAbs. Fold activation of IL2 reporter luciferase activity is presented as mean ± S.D. (n≥3; **** P≤0.0001).

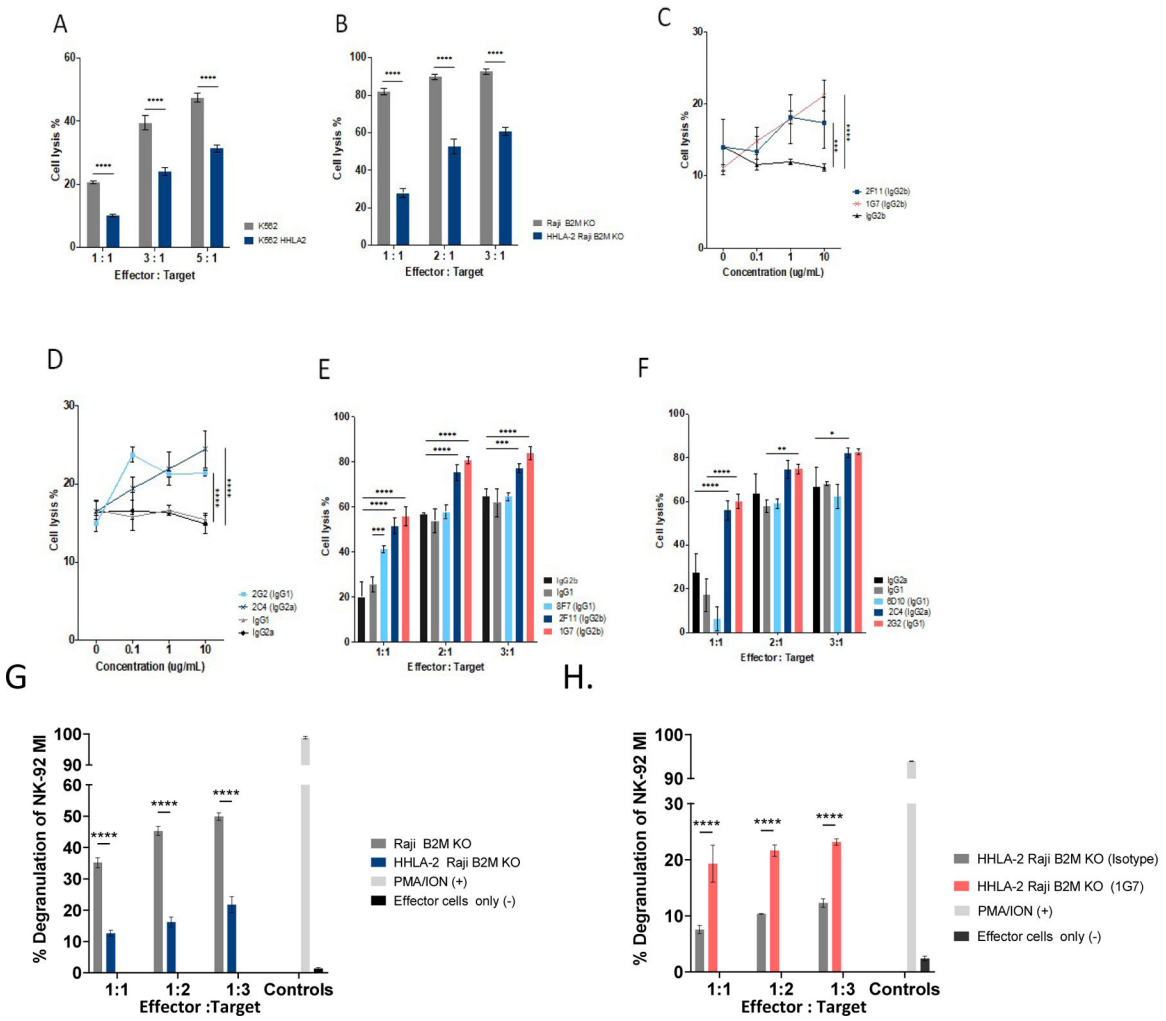

Figure 5: KIR3DL3 is an inhibitory receptor in NK cells and NK cytotoxicity is enhanced by HHLA2–KIR3DL3 blockade.

(**A**) NK-92MI cytotoxicity on K562 cells and K562 cells expressing HHLA2. (**B**) NK-92MI cytotoxicity on Raji cells harboring the β2M deletion (Raji-B2M KO cells) and Raji-B2M KO cells expressing HHLA2. (**C, D**) NK-92MI cytotoxicity on K562 cells expressing HHLA2 at an E:T ratio of 3:1 in the presence of (**C**) HHLA2 antibodies or (**D**) KIR3DL3 antibodies and isotype controls. (**E, F**) NK-92 MI cytotoxicity on Raji-B2M KO cells expressing HHLA2 at the indicated E:T ratios in presence of 10 ug/ml of (**E**) KIR3DL3 or (**F**) HHLA2 antibodies and isotype controls. (**G**) NK-92 MI cells were incubated with Raji B2M KO or with Raji B2M KO cells overexpressing HHLA2 at the indicated E:T ratios. Degranulation was measured as the % CD107a positive cells of the $CD56^+$ population. Controls were effector cells alone or effector cells with PMA/ION, which leads to total degranulation. (**H**) Enhanced degranulation of NK-92 MI cells targeting Raji B2M KO cells overexpressing HHLA2 in the presence of KIR3DL3 mAb (1G7) as compared with isotype control. N>3 replicates. Quantifications are presented as mean ± S.D. (N≥3; P≥0.05; *P≤0.05; **P≤0.01; ***P≤0.001; ****P≤0.0001).

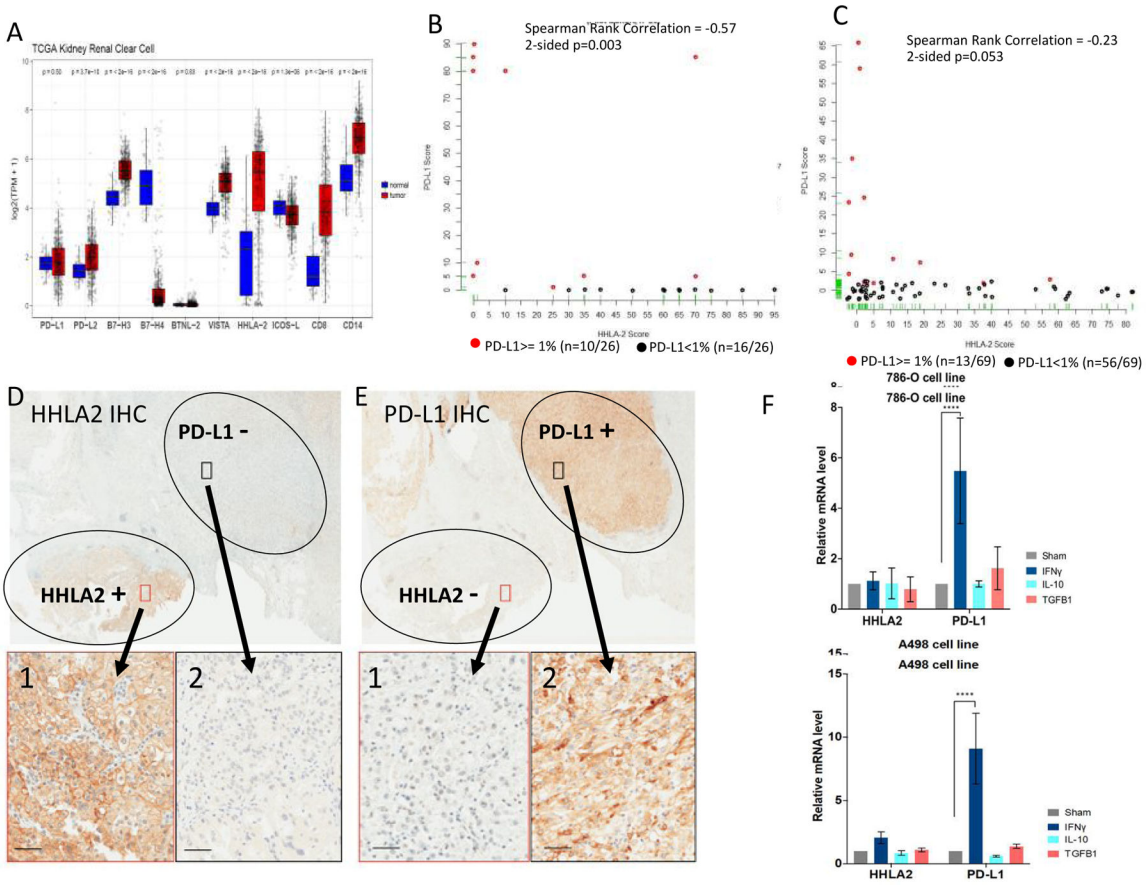

Figure 6: HHLA2 expression is non-overlapping with PDL1 expression.

(A) Expression levels of B7 family members in RCC as compared with normal kidney from TCGA samples. (**B, C**) Scatter plots of HHLA2 and PDL1 expression in ccRCC; sample scores for (**B**) pilot and **(C)** BMS-010 patient cohorts. (**D,E**) Sequential tissue sections from a ccRCC nephrectomy that expressed both HHLA2 and PDL1. (**D**) Staining for HHLA2 and (**E**) for PDL1, shows distinct, non-overlapping, areas of HHLA2 and PDL1 expression in the same tumor. Higher magnifications of the selected areas are also shown. The red box highlights region 1 of the tumor that is an HHLA2 positive area that is PDL1 negative; the black box highlights region 2 of the tumor that is a PDL1 positive area and HHLA2 negative. Scale bar: 50 μm. (**F**) RT-PCR analysis of HHLA2 and PDL1 expression in RCC cell lines (A498 and 786-O) after 48 h incubation with IFNγ, IL10 and TGFβ (10ng/ml). Quantifications are presented as mean ± S.D. (n≥3; two-way ANOVA; ****P≤0.0001).

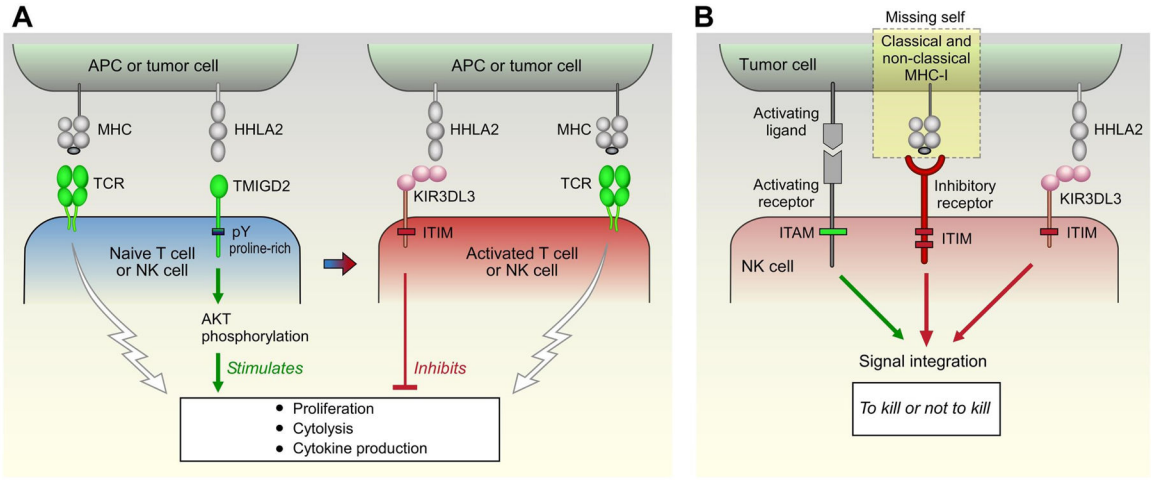

Figure 7: Model for HHLA2 pathway.

HHLA2 delivers an immune-stimulatory signal via TMIGD2 in naïve T cells or NK cells. (**A**) T-cell activation leads to a loss of TMIGD2 expression and gain of KIR3DL3. HHLA2 delivers an immune-inhibitory signal via KIR3DL3 in activated T cells. (**B**) NK-cell cytolytic activity is regulated by inhibitory and activating receptors. The inhibitory receptors include most KIRs, CD94/NKG2A, and LILRBI, which recognize MHC class I, E, and G, respectively. The activating receptors include NKG2D, NKp30, NKp44, NKp46, CD94/NKG2C, and TMIGD2 which recognize ULBP-1, MICA, MICB, B7-H6, HLA-E, HHLA2, and others. If tumors lose MHC class I expression (missing self), the inhibitory signal is reduced and the activating signals dominate, leading to tumor lysis by the NK cells. HHLA2 on tumors would be an inhibitory signal, independent of MHC class I, that inhibits lysis by KIR3DL3^{+} NK cells.